International Journal of Biological Macromolecules 130 (2019) 827–835

Contents lists available at ScienceDirect

International Journal of Biological Macromolecules

journal homepage: http://www.elsevier.com/locate/ijbiomac

Preparation and evaluation of *Bletilla striata* polysaccharide/graphene oxide composite hemostatic sponge

Junke Chen [a], Luyang Lv [a], Ying Li [a], Xiaodong Ren [b], Hao Luo [a], Yuanping Gao [a], Hengxiu Yan [a], Yanfang Li [a], Yan Qu [c], Lixin Yang [a], XiuJun Li [d], Rui Zeng [a,*]

[a] College of Pharmacy, Southwest Minzu University, Chengdu 610041, China
[b] Medical College, Guizhou University, Guiyang 550025, China
[c] College of Pharmacy, Chengdu University of Traditional Chinese Medicine, Chengdu 611137, China
[d] Department of Chemistry, University of Texas at El Paso, El Paso, TX 79968, USA

ARTICLE INFO

Article history:
Received 24 January 2019
Received in revised form 19 February 2019
Accepted 22 February 2019
Available online 23 February 2019

Keywords:
Bletilla striata polysaccharide
Graphene oxide
Hemostasis

ABSTRACT

Uncontrolled bleeding is an important cause of military and civilian casualties. GO has received more attention in the field of hemostasis. However, pure GO has various limitation in application due to its potential thrombosis, hemolytic and cytotoxicity. Herein, we present a simple, rapid and low-cost method to combine GO and natural polysaccharides by hydrogen bonding to prepare a new material *Bletilla striata* polysaccharide/graphene oxide composite sponge (BGCS). The BGCS was successfully synthesized and characterized by SEM, IR, RAMAN, XRD and Zeta potential analyzer analysis. The BGCS exhibited favorable biocompatibility. Besides, the porosity of BGCS was higher than 90% and showed good water absorption capacity. The results of whole blood coagulation evaluation showed that the BGCS can promote blood coagulation within 30 s without anticoagulant, showing excellent hemostatic effect. Further coagulation mechanism studies indicated that the surface of the BGCS possessed a high charge (-27.3 ± 0.9 mV) and showed strong platelet stimulation, the BGCS can also induce red blood cell aggregation, accelerate fibrin formation and accelerate blood coagulation. Therefore, the BGCS can stop bleeding within 50 s in rat-tail amputation models. The BGCS provides a new perspective for the safe application of GO in the field of trauma hemostasis.

1. Introduction

As reported, nearly 50% of deaths in the military are caused by hemorrhage [1]. In addition, excessive bleeding is also an important cause of death in natural disasters, traffic accidents, and traumatic bleeding among civilians [1–3]. Carbon aerogels exhibit 3D network, a high porosity structure and high specific surface area, they were synthetized from graphene oxide (GO), whose intrinsic properties make it has great potential in the biomedical applications, such as cancer therapy, tissue engineering, drug delivery, wound healing, biosensing and hemostasis [4–9]. The GO sheets cause strong aggregation in platelets by activating Src kinases and releasing calcium from intracellular stores, which is in a scale comparable to that triggered by thrombin [10]. In addition, activated platelets carry many other hemostatic factors that adhere to the wound surface and trigger the coagulation pathway [9], while graphene aerogels can rapidly absorb plasma, allowing blood cells to accumulate on the surface, further promoting blood coagulation on the wound surface [11]. However, the fatal shortcomings of GO, such as high hemolysis rate [12], potential thrombosis [10], and cytotoxicity [13], limit its application in hemostatic materials. This is related to the surface active chemical structure of GO with hydrophilic edges and hydrophobic basal plane [14,15]. Chemical crosslinking can alter the structural properties of polymeric materials [16]. Natural polysaccharide materials have been extensively studied for hemostasis due to their excellent biocompatibility and hemostatic activity [17,18]. In addition, natural polysaccharides can also be cross-linked with GO by covalent or noncovalent bonds to improve the chemical properties of GO [12,19,20].

Bletilla striata belongs to the Orchidaceae family, and has been widely used as an astringent hemostatic medicine in traditional Chinese medicine (TCM) for thousands of years. TCM holds that it can treat hematemesis, hemoptysis, traumatic hemorrhage and ulcerative carbuncles [21]. *Bletilla striata* polysaccharide (Bsp), traditionally used constituents of *Bletilla striata*, exhibited biocompatibility, biomedical activity and low toxicity [22]. The monosaccharide composition of Bsp is mainly glucose and mannose, so it is called glucomannan polymer [23–25]. Its possible chemical structure is shown in Fig. 1. This polysaccharide has shown effects on traumatic bleeding and alimentary canal hemorrhages, as well as increased platelet aggregation rate [26–28].

* Corresponding author.
E-mail address: rzeng@swun.edu.cn (R. Zeng).

https://doi.org/10.1016/j.ijbiomac.2019.02.137
0141-8130/

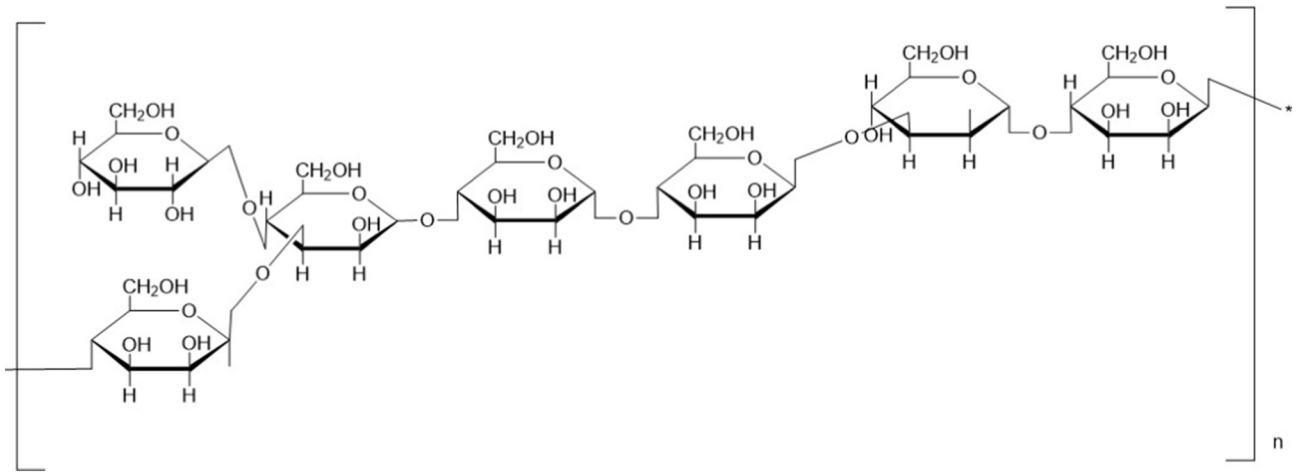

Fig. 1. The proposed structure of the *Bletilla striata* polysaccharide.

Besides, the abundant hydroxyl groups and long chains in the polysaccharide allow them to be structurally modified by crosslinking with other compounds to improve their fatal shortcomings [12]. Therefore, the Bsp is an excellent candidate for GO modification.

In this study, we present a simple and environmentally benign preparation of Bsp/GO composite sponge (BGCS) by a simple solution-mixing freeze-drying method. The BGCS has a stimulating effect with erythrocytes and platelets. Through the synergistic effect of stimulation and physical absorption, BGCS exerted strong hemostatic properties, and by the evaluation of the microstructure, physical and chemical properties, biocompatibility, hemostasis effects of the BGCS, providing direction for the safe use of GO in traumatic hemostasis.

2. Materials and methods

2.1. Materials

Graphite powder was purchased from Huayi Co., Shanghai, China. Tubers of *B. striata* were purchased from Sichuan Chinese Medicine Yinpian Co. Ltd. All other chemicals were of analytical grade.

2.2. Synthesis of graphene oxide (GO)

The graphene oxide solution was synthesized by a modified Hummers method [29]. Briefly, graphite powder (3 g) was pre-oxidized with phosphorus pentoxide (2.5 g) and potassium peroxydisulfate (2.5 g) in concentrated sulfuric acid (12 mL) at 80 °C for 4.5 h. The mixture was poured into distilled water (500 mL), filtered, washed and dried in vacuum oven. Next, the pre-oxidized graphite was added into concentrated sulfuric acid (120 mL) and under stirring potassium permanganate (15 g) was added slowly at 35 °C for 2 h. Then, the mixture was added into deionized water (250 mL) and stirred for another 2 h, followed by adding deionized water (500 mL) and hydrogen peroxide (20 mL). After filtration, the product was washed with 10% HCl aqueous solution (300 mL) and dialyzed for 7 days to remove the acid. At last, the viscous liquid was sonicated for 2 h to generate GO dispersion.

2.3. Preparation of Bletilla striata polysaccharide (Bsp)

Bletilla striata polysaccharide was prepared with some modifications following the methodology described by Qu et al. [30]. The tubers of *Bletilla striata* were over-dried, finely pulverized and sieved through a 30 mesh sieve. The powder was degreased in petroleum ether (5 mL/g, 70 °C) and refluxed twice with ethanol (10 mL/g, 95%) at 70 °C for 2 h. Next, the dryness powder was added to deionized water (40 mL/g). The mixture was then extracted twice at 70 °C for 2 h. Proteins were removed from the extracts using Sevag reagent (chloroform:butyl alcohol, 4:1 v/v), until the absorption of the solution at 260 nm and 280 nm was zero. Whereafter, the deproteinized solution was concentrated and four volumes of 95% ethanol were added to precipitate the polysaccharide. The precipitates were then collected by washing with dehydrated alcohol four times and drying to a constant weight.

2.4. Preparation and characterization of the BGCS

The Bsp crosslinked GO composite sponge (BGCS) was prepared by a simple solution-mixing freeze-drying method. Briefly, the Bsp was dissolved in deionized water and stirred for 12 h using a magnetic stirrer to obtain a 16 mg/mL solution, and the Bsp solution was added to 25 mL beaker. Then, the GO solution (8 mg/mL) was slowly added to the Bsp solution, and the final volume of the mixed solution was 15 mL with the solution was stirred for 4 h for crosslinking. Samples were frozen in the refrigerator at −80 °C for 12 h. The frozen BGCS were lyophilized in automated lyophilization mode (chamber pressure < 10 Pa, temperature < −55 °C) using freeze-drier (LGJ-18, Beijing Songyuanhuaxing Technology Develop Co., Ltd.), leading to the formation of the porous structure through the sublimation of water. By changing the mass ratio of Bsp to GO from 1:1, 5:1, 10:1 and 15:1, the BGCS, BGCS-5, BGCS-10 and BGCS-15 were prepared.

Scanning electron microscopy (SEM, Navo NanoSEM450) was used to observe the morphology of the BGCS. Infrared spectrometer (IR, Magna-IR 750, Nicolet), Raman spectroscopy (Raman, Horiba Labram HR Evolution) and X-ray diffraction (XRD, SmartLab (3)) were used to investigate the chemical composition and structure of the BGCS. The zeta potential (zetasizer nano ZS) was used to detect the negative potential of the BGCS. Besides, the GO sponges were prepared in the same method, by adding the same amount of water as the Bsp solution in the BGCS.

2.5. Porosity of composite sponges

Ethanol displacement method was applied to determine the porosity of the materials [2,31]. The samples were dried to a constant weight (W_S). Ethanol was fully filled into an empty bottle and the total weight was noted as W_1, the sample was immersed in the ethanol. Ultrasonic degassing was performed until the pores were ethanol saturated, with the bottle again filled with ethanol and weighed (W_2). The samples were quickly removed from the ethanol with forceps, then, the weight of the bottle and remaining ethanol (W_3) was measured. All samples

were triplicated, and porosity was calculated using the following formula:

$$\text{Porosity}\ (\%) = \frac{(W_2 - W_3 - W_s)}{(W_1 - W_3)} \times 100\%$$

2.6. Water absorption rate

After the composite sponges was immersed in deionized water adequately, the samples were tilted to 60° until no water droplets fell, and the excess liquid was removed using a filter paper, then weight (W_1) and the initial weight (W_0) of the sponge were recorded. The same sample was tested three times, and the water absorption rate was calculated using the following equation:

$$\text{Water absorption rate}\ (\%) = \frac{(W_1 - W_0)}{W_0} \times 100\%$$

2.7. Rat-tail amputation

The rat tail amputation model was used to characterize the hemostatic capacity of the specimens. Healthy male SD rats (250 ± 20 g, 7 weeks old), were treated and cared for in strict accordance with the National Research Council's Guide for the care and use of laboratory animals. Total rats were anesthetized with 10% chloral hydrate (0.5 mL per 100 g) before surgery. 6 cm length of the tail was cut and the GO, BGCS were pressed on the wound section with slight pressure. The hemostatic time (s) and the blood loss (g) were recorded, six parallel groups were tested to get the mean value. Commercial gauze sponge was used here as a control group.

2.8. Whole blood clotting evaluation

In order to evaluate the coagulation ability of BGCS, the SD rats' whole blood was used for *in vitro* coagulation time test. Total 50 μL volume of fresh blood was directly dropped onto eight test groups, including a blank, Blood+Ca^{2+} (4 μL $CaCl_2$ solution, 0.2 mol/L), commercial gauze sponge, the GO and BGCS-N (BGCS, BGCS-5, BGCS-10, BGCS-15) in glass dishes. Samples of equal size ($1 \times 1 \times 0.25\ cm^3$) were used. Each group reacted with blood for 30, 60, 120, and 240 s. After each time, 10 mL of distilled water was added slowly to stop the coagulation process and to dissolve the hemoglobin in free erythrocytes. The hemoglobin content in each supernatant was measured by UV–Visible Spectrophotometer (UV 2400, SDPTOP) at 542 nm and quantified by the following equation

$$\text{Hemoglobin absorbance} = I_s/I_r \times 100\%$$

where I_s is the absorbance of the resulting sample, and I_r is the absorbance of the reference value. As a reference value, the absorption of 50 μL fresh blood in 10 mL distilled water was measured. This experiment was repeated three times under the same conditions [6,11].

2.9. Hemolysis assay in vitro

Fresh anticoagulated blood (5 mL) from the healthy volunteer (female, 25 years old) was added into 10 mL phosphate buffered saline (PBS, pH 7.2–7.4) and centrifuged at 500*g* for 10 min to separate RBCs from serum. This purification step was repeated four times, and then the collected RBCs were diluted to 50 mL in PBS. To test the hemolytic activity of the BGCS, the GO and the Bsp, 0.2 mL of diluted RBCs was added to 0.8 mL of the material's suspension solutions in PBS at the range from 7.8 to 500 μg/mL. In order to get the sample's suspension

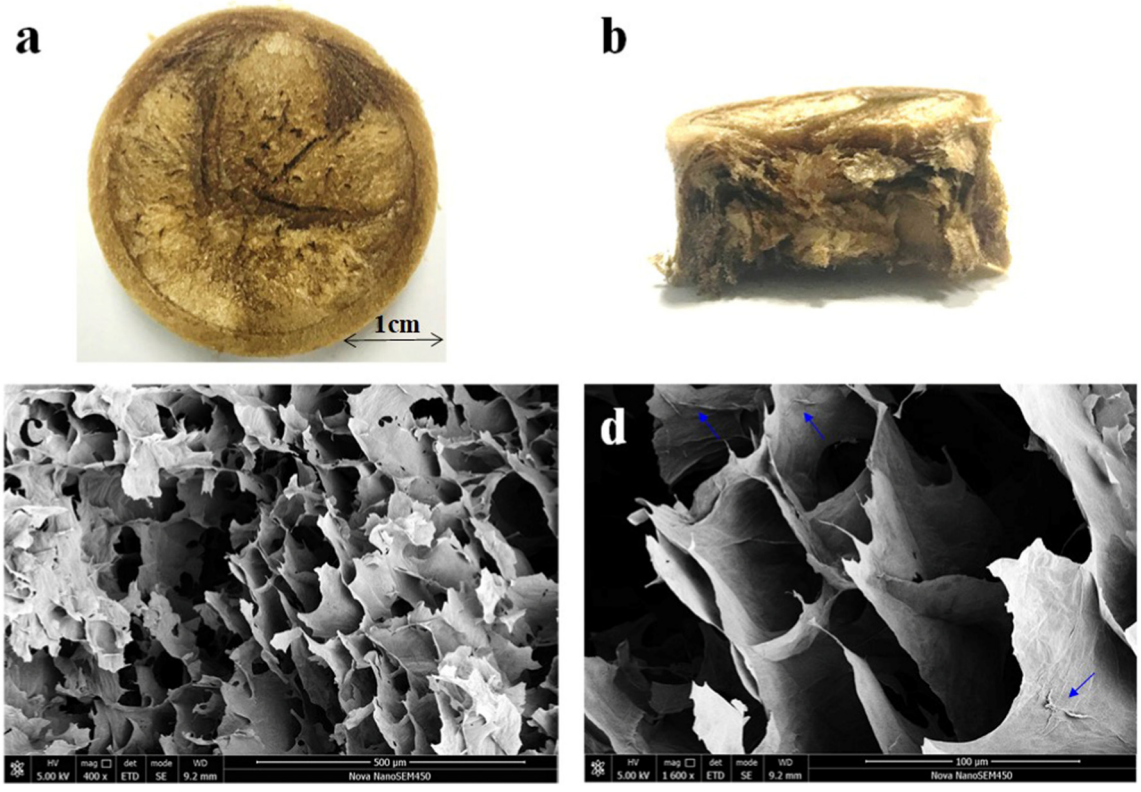

Fig. 2. Morphology of BGCS. (a) Photograph of the BGCS (3 cm diameter, 2 cm thickness). (b) Cross section of the BGCS. (c) SEM image of the interior porous structure of the BGCS. (d) The smooth cell wall of the porous structure.

solutions, the sample powders were added into PBS and sonicated for 2 h. Deionized water (+RBCs) and PBS (+RBCs) were chosen as positive and negative control, separately. All the samples were placed in a rocking shaker at 37 °C for 3 h. After incubation, these samples were centrifuged at 10,016*g* for 5 min. The hemoglobin absorbance was measured with a UV–Visible Spectrophotometer (UV2400, SDPTOP) at 540 nm. Percent hemolysis was calculated by the following formula:

$$\text{Percent hemolysis}(\%) = \frac{(\text{abs}_{s540nm} - \text{abs}_{n540nm})}{(\text{abs}_{p540nm} - \text{abs}_{s540nm})} \times 100\%$$

where abs_{s540nm}, abs_{n540nm}, and abs_{p540nm} are the hemoglobin absorbance of samples, negative controls and positive controls [12,32].

2.10. Cytotoxicity evaluation

The cytotoxicity of the BGCS towards the L-929 mouse fibroblast cell was evaluated by cell counting kit-8 assay (CCK-8, Dojindo). The cells were adjusted to 1×10^5 cells/mL in complete medium (CM), which consisted of 90% DEME medium, 10% fetal bovine serum (FBS) and 1% antibiotics (100 units mL^{-1} penicillin and 100 units mL^{-1} streptomycin). The cell suspension was added into 96-well plates (100 μL per well) and incubated for 24 h at 37 °C in a humidified air condition of 5% CO_2. Then, the cells were washed twice with PBS and different concentrations of the BGCS, the GO or the Bsp suspension in CM (15.63–250 μg/mL) were added into the plates to replace the original CM. Negative control cells did not receive any materials treatment. The background experiments were performed with the above method. After 24 h incubation, 10 μL CCK-8 solution was added to each well for 4 h incubation, 80 μL supernatant was transferred to another 96-well plate. The optical density (OD) of the mixture solutions was measured at 450 nm with a reference of 655 nm, using an iMark microplate reader. The cell viability was expressed as a percentage as the following formula:

$$\text{Cell viability}\ (\%) = \frac{(\text{OD}_{test} - \text{OD}_{blank})}{(\text{OD}_{negative\ control} - \text{OD}_{blank})} \times 100\%$$

where OD_{test}, OD_{blank}, $\text{OD}_{negative\ control}$ are the optical density values from sample wells, negative control wells and the background wells.

2.11. Interfacial interaction between blood cells and the BGCS

For blood cells and platelet selective adhesion test, a small piece of the BGCS ($1 \times 1\ cm^2$, 0.25 cm thickness) was immersed in 10 mL PBS and equilibrated for 2 h at 37 °C. 0.5 mL of ACD-whole blood or PRP was added and incubated for another 1 h at 37 °C. Then, the sample was rinsed three times with PBS and immobilized with 2.5% glutaraldehyde for 2 h at 4 °C. The samples were then dehydrated with 50%, 60%, 70%, 80%, 90% and 100% ethanol for 10 min and the freeze-drying and metal-spraying processes were completed prior to SEM observation. [33].

For blood cells morphology observation, 50 μL ACD-whole blood was added onto the BGCS (3 cm diameter, 2 cm thickness) surface, and the material was incubated for 3 min at 37 °C. The samples were treated with the above-mentioned method prior to SEM observation [34,35].

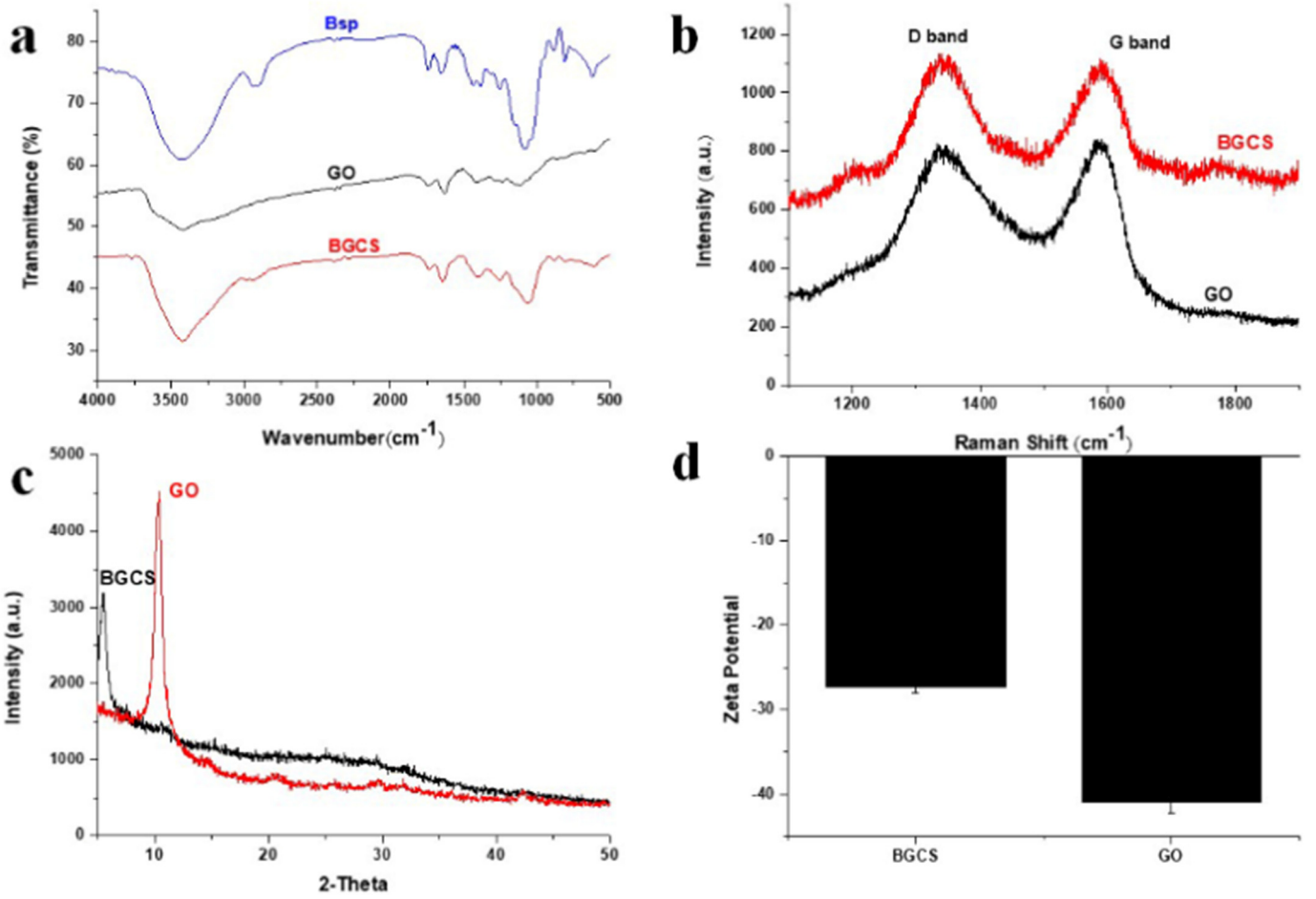

Fig. 3. Characterization of the BGCS. (a) FT-IR spectra of the Bsp, the GO and the BGCS. (b) Raman, (c) XRD and (d) Zeta potential tests of the GO and the BGCS sponge. Data values corresponded to mean ± SD (n = 3).

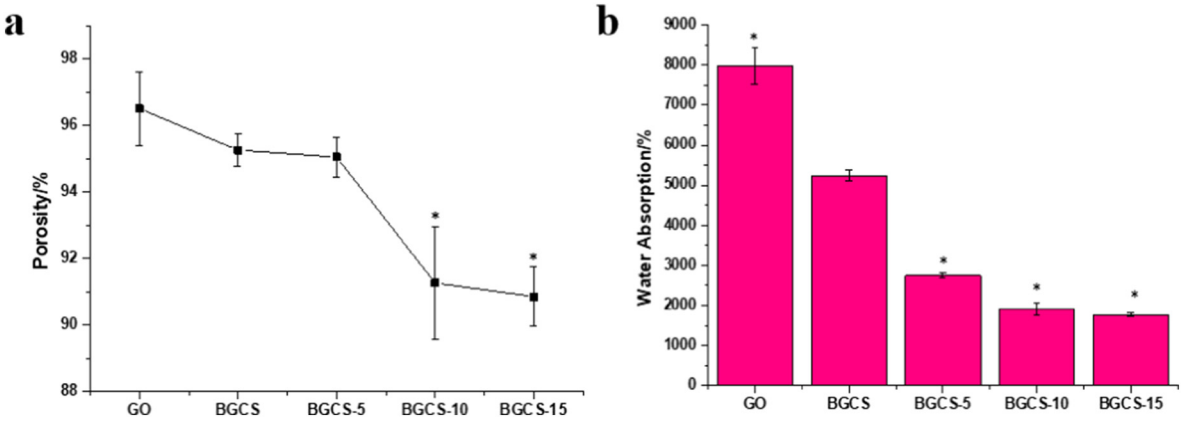

Fig. 4. The porosity (a) and the water absorption (b) of the GO and the BGCS-N sponges. *P < 0.05 compared with the BGCS. Data values corresponded to mean ± SD (n = 3).

3. Results and discussions

3.1. Material characterization

Fig. 2a shows the typical BGCS hemostatic sponge prepared *via* Bsp crosslinked GO aerogel, and the aerogel crosslinked each other to form a uniform, fluffy, porous cavity structure (Fig. 2b). As shown in Fig. 2c and d, the BGCS exhibits a heterogeneous porous structure having a large number of cavities, measuring from tens to hundreds of micrometers. The network maintained a strong interconnection between the layers, and the surface of the sponge is rough and has a large number of wrinkled textures (marked with the blue arrows), suggesting that the Bsp may adhere to the GO, and they were intertwined by hydrogen bonding.

Many investigations confirmed the abundance of oxygen-containing groups in the GO [36,37]. The hydrophilic oxygenated functional groups on the surface of the GO play a key role in improving the compatibility between GO and the polymer matrix. As shown in Fig. 3a, the signals at 3428.04, 1739.48, 1631.48, 1406.54, 1235.51, 1106.54 cm^{-1} are characteristic of the GO [37,38]. The —OH/—COOH groups were reflected by the peak at 3428.04 cm^{-1}, the peak at 1739.48 cm^{-1} indicated the presence of C═O, the typical C═C signal was detected at 1631.48 cm^{-1}, the C—O bonds were indicated by the peak at 1406.54 cm^{-1} (carboxyl C—O), 1235.51 cm^{-1} (epoxy C—O), 1106.54 cm^{-1} (epoxy or alkoxy C—O). Besides, from the FTIR spectra of the Bsp (Fig. 2a), the strong and broad peak at 3430.74 cm^{-1} corresponded to the stretching vibration of —OH, the peak at 2937.93 cm^{-1} indicated the asymmetric stretching vibration of C—H, the bands at 1648.84 cm indicated the presence C═O asymmetric stretching vibration absorption bands, and the peak at 1743.47 cm^{-1} indicated the presence of uronic acids in Bsp. The characteristic absorption band of furan glycosides is at 1078.86 cm^{-1}. The signals at 811.06 cm^{-1} and 883.77 cm^{-1} stand for mannose residues [2,30]. When Bsp was added into the GO, the peak at 3428.04–3419.17 cm^{-1} (O—H stretching vibrations), 1739.48–1731.78 cm^{-1} (C═O of carboxylic acid), 1631.48–1644.98 cm^{-1} (aromatic C═C), 1406.54–1395.33 cm^{-1} (carboxyl C—O), 1235.51–1249.53 cm^{-1} (epoxy C—O), 1106.54–1056.07 cm^{-1} (epoxy or alkoxy C—O) sharpened, suggesting that Bsp interacted with GO through intermolecular hydrogen bonds, and Bsp and GO should have good miscibility [39].

The Raman spectra of GO and BGCS are shown in Fig. 3b, which show similar peak structures, *e.g.*, the G band (E2g mode of sp^2 carbon atoms) was at approximately 1588 cm^{-1}, and the D band was at about 1341 cm^{-1} (symmetry A1g mode). The ID to IG ratio of the BGCS is 1.01, which is higher than that of the GO (0.98), indicating that the combination of the Bsp and the GO increases the disorder of the material. Compared with GO, the G band of BGCS exhibits a blue shift from 1588 cm^{-1} to 1592 cm^{-1} due to the higher amount of sp^2 carbon

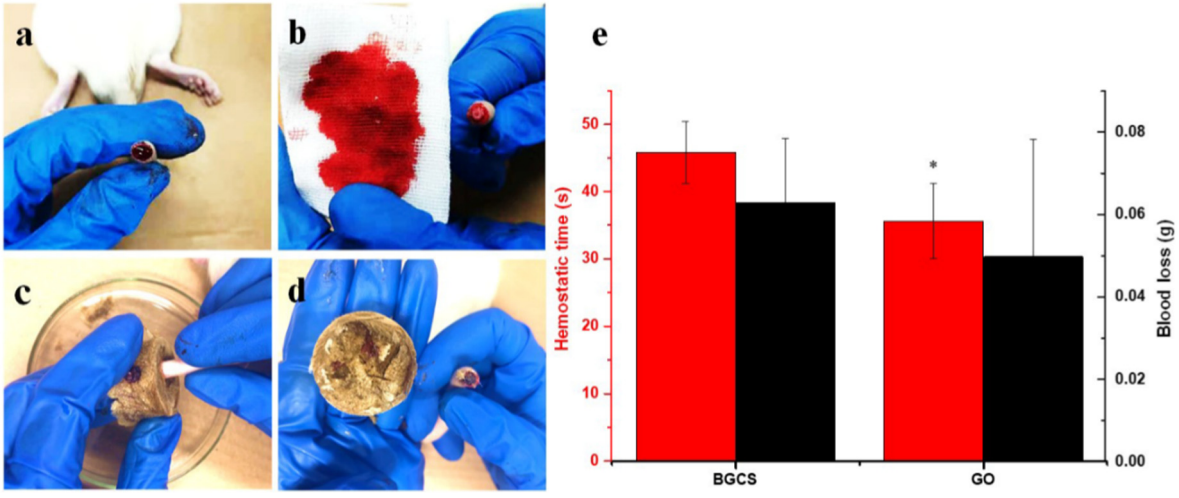

Fig. 5. Evaluation on the hemostatic performance of the BGCS. (a) Cutting the tail of the rat and bleeding. (b) 10 min application of gauze sponge resulted in continued bleeding. (c) BGCS was pressed on the wound. (d) Hemostasis was achieved by the BGCS. (e) The hemostatic time and blood loss of the GO and the BGCS sponges. Data values corresponded to mean ± SD, n = 6. *P < 0.05 compared with the GO sponge.

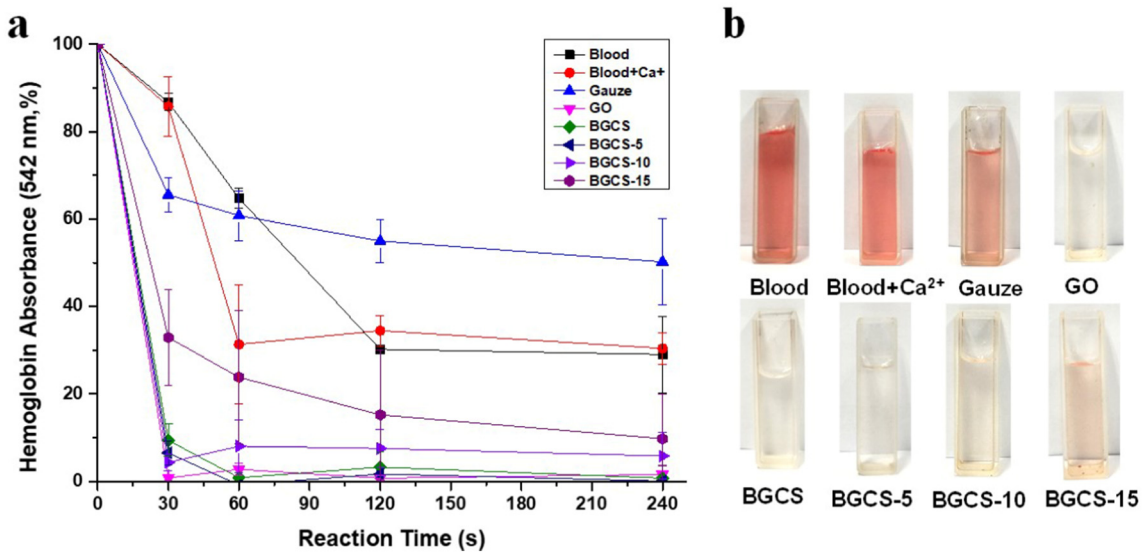

Fig. 6. Whole blood clotting (a) *in vitro* dynamic whole-blood clotting evaluation of the GO, the BGCS-N and controls (Ca^{2+} and Gauze); data values corresponded to mean ± SD (n = 3). (b) Photographs of the corresponding aqueous solutions of hemoglobin after 30 s.

atom content in BGCS, and those sp^2 carbon atoms were produced by partial reduction of oxygen-containing functional groups in GO [40]. Besides, the structure of the BGCS was further investigated by XRD (Fig. 3c). When the GO aerogel was crosslinked by the Bsp, the characteristic diffraction angle (2θ) of GO decreased from 10.4° to 5.43°, which indicates that the interlayer spacing increased from 0.85 nm to 1.62 nm, and the BSP is successfully inserted into the GO layer to form a special sandwich structure.

The zeta potential measurement confirmed the surface charge density of the GO and the BGCS. As shown in Fig. 3d, the electric negative potential of the GO was −40.9 ± 1.7 mV, and the BGCS (−27.3 ± 0.9 mV) was lower than the GO. We deduced that the property changes would reduce the thrombosis toxicity of GO [10]. Similarly, the strong negative charges in BGCS can activate blood clotting factors in platelets, and accelerate blood coagulation [41,42].

3.2. Porosity and water absorption of the sponges

The higher porosity facilitates the hemostatic material to absorb exudates from the wound surface and commence gas exchange. As shown in Fig. 4a, the porosity of the GO sponge was 96.5 ± 1.11%, and the BGCS was 95.3 ± 0.49%, but the change was not statistically significant. With the amount of Bsp further increases, the porosity of the composite sponge decreases. But the porosity of all sponges exceeds 90%, and the porosity of the sponges is a key factor in determining the fluid absorption capacity [2].

Medical hemostatic materials should have good liquid absorption capacity, which can accelerate blood coagulation by rapidly absorbing exudate and plasma on the wound surface [2,43]. Fig. 4b presents that the water absorption of the GO is 7972.81 ± 451.01%. The absorption capacity of the material is dose dependent with Bsp, and increasing the dose of Bsp (the ratio of Bsp/GO from 1:1 to 15:1, m/m) weaken the absorption capacity of the materials. It is possible that the Bsp crosslinks with the GO, making the molecular chain tighter and the surface negative charges weakened, thus decreasing the water absorption capacity [44]. Besides, the water absorption of the sponges was also affected by the porosity, and its porous structure was also an important factor affecting the water absorption capacity [45]. The BGCS (1:1, m/m) whose water absorption is 5239.86 ± 129.65%, possessed the best absorption capacity.

3.3. In vivo hemostatic efficacy

Rat-tail amputation models are a usual bleeding model for evaluating the hemostatic material [11,46]. The gauze sponge (Fig. 5b) was used as the control group to directly press on the wound surface. The gauze did not promote blood coagulation, and even after 10 min, the blood could only prevent from flowing out by pressing [47]. However, when the BGCS was pressed slightly onto the wound (Fig. 5c), the BGCS could quickly absorb blood and rapidly formed a clot at the interface to stop bleeding (Fig. 5d). As shown in Fig. 5e, among the six parallel bleeding experiments, the mean bleeding time was 45.9 ± 4.6 s, and the bleeding time of the GO was 35.6 ± 5.6 s, although the BGCS was slightly lower than the GO, the BGCS still could play an excellent role in hemostasis. Besides, the mean blood loss of BGCS was 0.063 ± 0.016 g, although it was slightly higher than the blood loss of GO (0.050 ± 0.028 g), there was no significant difference (P > 0.05).

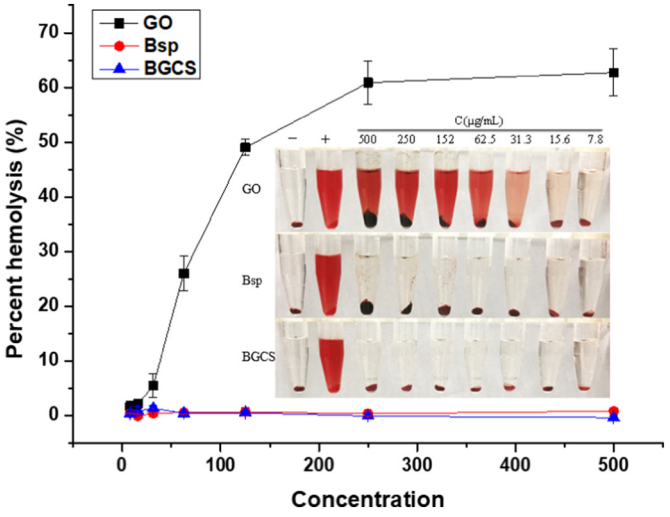

Fig. 7. Hemolysis assays for the BGCS, the GO and the Bsp. Inset: the photographs show no significant hemoglobin leakage from the BGCS approached RBSs compared to the positive control. (+) and (−) symbols represent positive and negative control group, respectively. Data values corresponded to mean ± SD (n = 3).

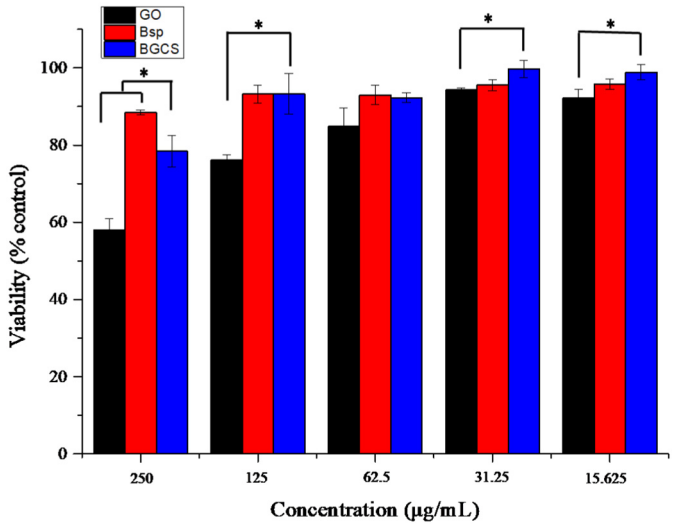

Fig. 8. Cell viability of L-929 mouse fibroblast cell determined from CCK-8 assay after 24-h exposure to different concentrations (15.63–250 μg/mL) of the GO, the BGCS and the Bsp. Data represented mean ± SD. *P < 0.05 denotes significant differences compared with the BGCS.

Simultaneously, the hemostatic performance of the other BGCS-N was investigated. The hemostasis time of BGCS-5 and BGCS-10 was extended to 54.8 ± 11.6 s and 113.8 ± 20.8 s. With the increase of Bsp, the hemostasis time of the material is prolonged. We inferred that the increased hemostatic time of BGCS-N related to their porosity and surface charge, thus ensuring the liquid absorption capacity and higher charge density of the BGCS is essential for rapid hemostasis.

3.4. In vitro dynamic whole-blood clotting

The dynamic whole-blood clotting study was conducted to assess the hemostatic potential of BGCS *in vitro*. In this assay, the same amount of fresh blood without anticoagulant was directly added to the samples, gauze (negative control) and Ca^{2+} (a coagulation factor, positive control). Test samples as coagulant material, was interacted with fresh blood and their performance was observed by an ultraviolet spectrophotometer at 542 nm. As shown in Fig. 6a, during the whole blood clotting test, the GO and the BGCS-N showed lower absorbance values than the control groups (blood, gauze and blood + Ca^{2+}) and thus more blood clotting. In the first 30 s of contact with the whole blood, the absorbance value of the GO and the BGCS-N were far lower than the control groups, the difference in hemoglobin concentration in the supernatant was significant (Fig. 6b). For all control groups, the blood began to coagulate after about 60 s. The blood in the GO and the BGCS-N coagulated almost completely at 30 s, but as the amount of Bsp increases, the hemoglobin absorbance increases, and the coagulation effect of the BGCS (1–5) is comparable to that of GO. Therefore, it is probable that the BGCS can accelerate blood clotting when the blood coagulant had not yet functioned. We deduced that the BGCS absorb plasma, allowing rapid blood clotting through the activation of the intrinsic coagulation system and surface charge of the material [6].

3.5. In vitro hemolysis assay

Hemolysis assay is a universal method to evaluate the *in vitro* blood compatibility of materials [48]. Direct exposure of the GO to the RBCs solution resulted in dose-dependent developing of hemoglobin (Fig. 7), about 250 μg/mL dose of GO caused 60.9 ± 4.0% hemolysis. This result confirmed that the GO has bio-toxicity and may cause thrombosis [10]. Conversely, the RBCs treated with the same dose of the BGCS did not show hemolysis. When the dosage of the BGCS was up to 500 μg/mL, the max rate is no >2%. Besides, Liao et al. [12] confirmed that the light absorption by the GO is not an important issue in the hemolysis assay, so the hemolysis ratio of the Bsp crosslinked GO is much lower than the hemolysis ratio of the GO.

3.6. Cytotoxicity evaluation

Usually, MTT is often used to predict the toxicity of materials, but the GO could spontaneously reduce MTT thus resulting in a false positive signal [12]. So the effect of the GO, the BGCS and the Bsp on L929 cell viability was assessed using the CCK-8 assay. As shown in Fig. 8, the L929 cells were cultured with different concentrations (15.63–250 μg/mL) of the GO, BGCS and Bsp for 24 h. Increasing GO concentration from 15.63 to 250 μg/mL dose-dependently decreased cell viability from 92.19 ± 2.33% to 57.96 ± 3.03%, with the cell viability of the BGCS-treated cells significantly ($P < 0.05$) increased as compared with that of the GO-treated cells. At a concentration from 15.63 to 250 μg/mL, the cell viability of the BGCS-treated cells decreased from 98.86 ± 1.96% to 78.41 ± 4.04%. Therefore, Bsp crosslinked with GO can reduce its cytotoxicity. Besides, there was no difference of cell viability ($P > 0.05$) between the BGCS and the Bsp except for 250 μg/mL.

3.7. The interaction between the interface of BGCS and blood cells

GO could not directly contact with blood, but Bsp-modified GO materials could be in direct contact with blood and exert excellent hemostatic properties. To elucidate the hemostatic mechanism, morphological studies of the hemocytes and platelets on the BGCS were performed according to the literature methods [9,42]. Firstly, when the BGCS was incubated with whole blood in PBS, the BGCS does not affect the morphology of blood cells, because none of the blood cells are deformed or aggregated on the surface of the BGCS (Fig. 9a). This result is consistent with the hemolysis assay. By contrast, when BGCS was incubated with PRP in PBS, it was clearly observed that platelets

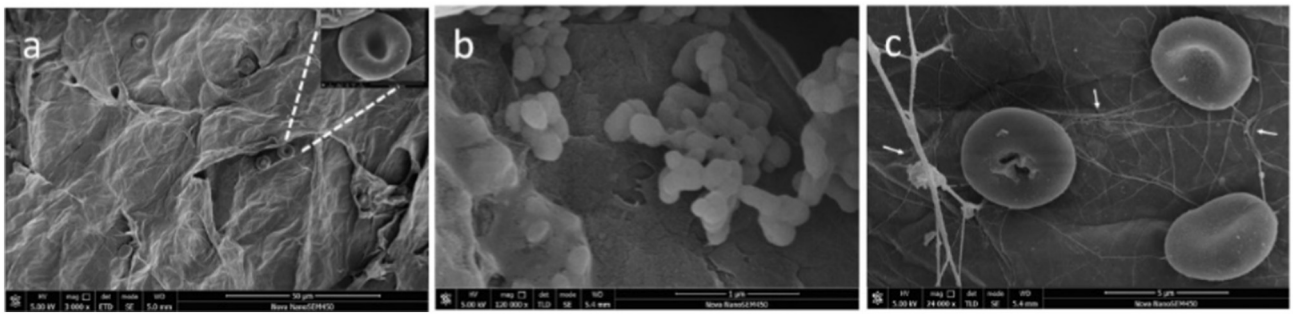

Fig. 9. SEM images of interaction between blood cells and the BGCS. The blood cells (a) and the platelets (b) selectively adhere on the surface of the BGCS. (c) A droplet of whole blood was directly dropped onto the BGCS, hemocytes were forced to adhere to it. The white arrow in the figure represents the fibrin formed.

aggregated on the surface of BGCS and changed their regular shape (Fig. 9b). Besides, when a droplet of whole blood was directly dropped onto the surface of BGCS, the plasma was rapidly absorbed into the BGCS, and a large number of blood cells were accumulated on the surface to form a micron-sized blood clot, as shown in Fig. 9c. The RBCs that can be observed were covered and crosslinked with the formed fibrin (the white arrow). The presence of RBCs during clot formation increased the resistance of the clot to fibrinolysis, increased the heterogeneity of the fibrin network, and enhanced the stability of the blood clot [49].

4. Conclusions

In summary, the BGCS was proven to be a safe, effective and low-cost potential hemostatic agent. BGCS can stop bleeding within 50 s in the rat-tail amputation models. Its high porosity sponge structure absorbs blood quickly, and the high surface charge (-27.3 ± 0.9 mV) can effectively activate platelets and accelerate the formation of fibrin. As the GO contains rich hydroxyl groups and epoxy groups on its surface, the GO and Bsp are uniformly and tightly linked by hydrogen bonding when they are mixed. This stable structure assures the biosafety of the BGCS. According to the previous reports, the GO destructed hemocytes, caused cytotoxicity and even formed a thrombus, while the BGCS can significantly improve these conditions. Therefore, the BGCS shows great potential in the field of wound hemostasis.

Acknowledgements

This work was supported by the National Natural Science Foundation of China (81603309), National Key Research and Development Program of China (2017YFC1700705), Sichuan Provincial Scholars for Science and Technology Activities for Overseas Researchers (2018-68), Research Project of Sichuan Province Department (2019YFS0174 and 2018JY0069), the Key Projects of Central Universities (2018NZD18), NIH/NIAID (R21AI107415), and U.S. NSF-PREM Program (DMR 1205302 and 1827745).

References

[1] C. Feng, J. Li, G.S. Wu, Y.Z. Mu, M. Kong, C.Q. Jiang, X.J. Cheng, Y. Liu, X.G. Chen, Chitosan-coated diatom silica as hemostatic agent for hemorrhage control, ACS Appl. Mater. Interfaces 8 (2016) 34234–34243.
[2] C. Wang, W. Luo, P. Li, S. Li, Z. Yang, Z. Hu, Y. Liu, N. Ao, Preparation and evaluation of chitosan/alginate porous microspheres/Bletilla striata polysaccharide composite hemostatic sponges, Carbohydr. Polym. 174 (2017) 432–442.
[3] H.B. Alam, D. B., J.A. DaCorta, P. Rhee, Hemorrhage control in the battlefield: role of new hemostatic agent, Mil. Med. 170 (2005) 63–69.
[4] O. Akhavan, E. Ghaderi, S. Aghayee, Y. Fereydooni, A. Talebi, The use of a glucose-reduced graphene oxide suspension for photothermal cancer therapy, J. Mater. Chem. 22 (2012) 13773–13781.
[5] S. Goenka, V. Sant, S. Sant, Graphene-based nanomaterials for drug delivery and tissue engineering, J. Control. Release 173 (2014) 75–88.
[6] C. Mellado, T. Figueroa, R. Baez, R. Castillo, M. Melendrez, B. Schulz, K. Fernandez, Development of graphene oxide composite aerogel with proanthocyanidins with hemostatic properties as a delivery system, ACS Appl. Mater. Interfaces 10 (2018) 7717–7729.
[7] X. Yan, F. Li, K.D. Hu, J. Xue, X.F. Pan, T. He, L. Dong, X.Y. Wang, Y.D. Wu, Y.H. Song, W.P. Xu, Y. Lu, Nacre-mimic reinforced Ag@reduced graphene oxide-sodium alginate composite film for wound healing, Sci. Rep. 7 (2017) 13851–13861.
[8] E. Morales-Narváez, A. Merkoçi, Graphene oxide as an optical biosensing platform, Adv. Mater. 24 (2012) 3298–3308.
[9] G. Li, Y. Liang, C. Xu, H. Sun, L. Tao, Y. Wei, X. Wang, Polydopamine reinforced hemostasis of a graphene oxide sponge via enhanced platelet stimulation, Colloids Surf. B: Biointerfaces 174 (2018) 35–41.
[10] S.K. Singh, M.K. Singh, M.K. Nayak, K. Sharda, S. Siddhartha, J.J.A. Grácio, D. Debabrata, Thrombus inducing property of atomically thin graphene oxide sheets, ACS Nano 5 (2011) 4987–4996.
[11] K. Quan, G. Li, D. Luan, Q. Yuan, L. Tao, X. Wang, Black hemostatic sponge based on facile prepared cross-linked graphene, Colloids Surf. B: Biointerfaces 132 (2015) 27–33.
[12] K.H. Liao, Y.S. Lin, C.W. Macosko, C.L. Haynes, Cytotoxicity of graphene oxide and graphene in human erythrocytes and skin fibroblasts, ACS Appl. Mater. Interfaces 3 (2011) 2607–2615.
[13] M.C. Duch, G.R.S. Budinger, T.L. Yu, S. Soberanes, D. Urich, S.E. Chiarella, L.A. Campochiaro, A. Gonzalez, N.S. Chandel, M.C. Hersam, Minimizing oxidation and stable nanoscale dispersion improves the biocompatibility of graphene in the lung, Nano Lett. 11 (2011) 5201–5207.
[14] K. Jaemyung, L.J. Cote, K. Franklin, Y. Wa, K.R. Shull, H. Jiaxing, Graphene oxide sheets at interfaces, J. Am. Chem. Soc. 132 (2010) 8180–8186.
[15] L. Fan, H. Ge, S. Zou, Y. Xiao, H. Wen, Y. Li, H. Feng, M. Nie, Sodium alginate conjugated graphene oxide as a new carrier for drug delivery system, Int. J. Biol. Macromol. 93 (2016) 582–590.
[16] W. Zhao, R.W.N. Nugroho, K. Odelius, U. Edlund, C. Zhao, A.-C. Albertsson, In situ cross-linking of stimuli-responsive hemicellulose microgels during spray drying, ACS Appl. Mater. Interfaces 7 (2015) 4202–4215.
[17] X. Song, K. Wang, C.-Q. Tang, W.-W. Yang, W.-F. Zhao, C.-S. Zhao, Design of carrageenan-based heparin-mimetic gel beads as self-anticoagulant hemoperfusion adsorbents, Biomacromolecules 19 (2018) 1966–1978.
[18] X. Huang, R. Wang, T. Lu, D. Zhou, W. Zhao, S. Sun, C. Zhao, Heparin-like chitosan hydrogels with tunable swelling behavior, prolonged clotting times, and prevented contact activation and complement activation, Biomacromolecules 1 (2016) 4011–4020.
[19] L.D. Young, K. Zehedina, L. Ji-Hoon, L. Yong-Kyu, I. Insik, Blood compatible graphene/heparin conjugate through noncovalent chemistry, Biomacromolecules 12 (2011) 336–341.
[20] D. Depan, B. Girase, J.S. Shah, R.D.K. Misra, Structure–process–property relationship of the polar graphene oxide-mediated cellular response and stimulated growth of osteoblasts on hybrid chitosan network structure nanocomposite scaffolds, Acta Biomater. 7 (2011) 3432–3445.
[21] X. He, X. Wang, J. Fang, Z. Zhao, L. Huang, H. Guo, X. Zheng, Bletilla striata: medicinal uses, phytochemistry and pharmacological activities, J. Ethnopharmacol. 195 (2016) 20–38.
[22] Y. Song, R. Zeng, L. Hu, K.G. Maffucci, X. Ren, Y. Qu, In vivo wound healing and in vitro antioxidant activities of Bletilla striata phenolic extracts, Biomed. Pharmacother. 93 (2017) 451–461.
[23] Y. Wang, D. Liu, S. Chen, Y. Wang, H. Jiang, H. Yin, A new glucomannan from Bletilla striata: structural and anti-fibrosis effects, Fitoterapia 92 (2014) 72–78.
[24] Q. Peng, M. Li, F. Xue, H. Liu, Structure and immunobiological activity of a new polysaccharide from Bletilla striata, Carbohydr. Polym. 107 (2014) 119–123.
[25] W. Yu, J. Liu, L. Qiu, Y. Wang, C. Wang, Two natural glucomannan polymers, from Konjac and Bletilla, as bioactive materials for pharmaceutical applications, Biotechnol. Lett. 37 (2015) 1–8.
[26] W. Wang, M. Cheng, J. Gao, X. Zhang, Study on hemostasis of Bletilla striata hemostatic sponge, J. Pharm. Pract. 34 (2016) 32–35.
[27] Y.U. Linhua, X. Nie, H. Pan, L. Shuang, D. Zhang, K. Bian, Diabetes mellitus ulcers treatment with Bletilla striata polysaccharide, Zhongguo Zhong Yao Za Zhi 36 (2011) 1487–1491.
[28] B. Lu, Y.M. Xu, H.M. Zhang, T.J. Li, Y. Qiu, Effects of different extracts from Bletilla colloid on rabbit platelet aggregation, Pharm. J. Chinese People's Liberation Army 05 (2005) 330–332.
[29] W.S. H. Jr., R.E. Offeman, Preparation of graphitic oxide, J. Am. Chem. Soc. 80 (1958) 1339.
[30] Y. Qu, C. Li, C. Zhang, R. Zeng, C. Fu, Optimization of infrared-assisted extraction of Bletilla striata polysaccharides based on response surface methodology and their antioxidant activities, Carbohydr. Polym. 148 (2016) 345–353.
[31] J.Y. Liu, Y. Li, Y. Hu, G. Cheng, E. Ye, C. Shen, F.J. Xu, Hemostatic porous sponges of cross-linked hyaluronic acid/cationized dextran by one self-foaming process, Mater. Sci. Eng. C 83 (2018) 160–168.
[32] G. Li, K. Quan, Y. Liang, T. Li, Q. Yuan, L. Tao, Q. Xie, X. Wang, Graphene-montmorillonite composite sponge for safe and effective hemostasis, ACS Appl. Mater. Interfaces 8 (2016) 35071–35080.
[33] R. Gu, W. Sun, H. Zhou, Z. Wu, Z. Meng, X. Zhu, Q. Tang, J. Dong, G. Dou, The performance of a fly-larva shell-derived chitosan sponge as an absorbable surgical hemostatic agent, Biomaterials 31 (2010) 1270–1277.
[34] C. Dai, Y. Yuan, C. Liu, J. Wei, H. Hong, X. Li, X. Pan, Degradable, antibacterial silver exchanged mesoporous silica spheres for hemorrhage control, Biomaterials 30 (2009) 5364–5375.
[35] M.F. Shih, M.D. Shau, M.Y. Chang, S.K. Chiou, J.K. Chang, J.Y. Cherng, Platelet adsorption and hemolytic properties of liquid crystal/composite polymers, Int. J. Pharm. 327 (2006) 117–125.
[36] Z. Rao, H. Ge, L. Liu, C. Zhu, L. Min, M. Liu, L. Fan, D. Li, Carboxymethyl cellulose modified graphene oxide as pH-sensitive drug delivery system, Int. J. Biol. Macromol. 107 (2018) 1184–1192.
[37] L. Chen, C. Wang, H. Li, X. Qu, S.T. Yang, X.L. Chang, Bioaccumulation and toxicity of (13)C-skeleton labeled graphene oxide in wheat, Environ. Sci. Technol. 51 (2017) 10146–10153.
[38] M. Mohandoss, S.S. Gupta, A. Nelleri, T. Pradeep, S.M. Maliyekkal, Solar mediated reduction of graphene oxide, RSC Adv. 7 (2017) 957–963.
[39] M. Yadav, K.Y. Rhee, I.H. Jung, S.J. Park, Eco-friendly synthesis, characterization and properties of a sodium carboxymethyl cellulose/graphene oxide nanocomposite film, Cellulose 20 (2013) 687–698.
[40] Y. Qi, M. Yang, W. Xu, S. He, Y. Men, Natural polysaccharides-modified graphene oxide for adsorption of organic dyes from aqueous solutions, J. Colloid Interface Sci. 486 (2017) 84–96.
[41] M. Miyamoto, S. Sasakawa, T. Ozawa, H. Kawaguchi, Y. Ohtsuka, Platelet aggregation induced by latex particles. I. Effects of size, surface potential and hydrophobicity of particles, Biomaterials 10 (1989) 251–257.
[42] K. Quan, G. Li, L. Tao, Q. Xie, Q. Yuan, X. Wang, Diaminopropionic acid reinforced graphene sponge and its use for hemostasis, ACS Appl. Mater. Interfaces 8 (2016) 7666–7673.

[43] P. Zahedi, I. Rezaeian, S.O. Ranaei-Siadat, S.H. Jafari, P. Supaphol, A review on wound dressings with an emphasis on electrospun nanofibrous polymeric bandages, Polym. Adv. Technol. 21 (2010) 77–95.
[44] R. Barbucci, A. Magnani, M. Consumi, Swelling behavior of carboxymethylcellulose hydrogels in relation to cross-linking, pH, and charge density, Macromolecules 33 (2000) 7475–7480.
[45] W. Ye, H. Zhong, X. Li, X. Wang, R. Sun, Polyelectrolyte sponge reinforced with organic rectorite and silver nanoparticles, Curr. Nanosci. 9 (2013) 742–746.
[46] C. Zhang, R. Zeng, Z. Liao, C. Fu, H. Luo, H. Yang, Y. Qu, Bletilla striata micron particles function as a hemostatic agent by promoting rapid blood aggregation, Evid. Based Complement. Alternat. Med. (2017) 1–8.
[47] S. Anita, J.C. Fang, P. Sravanthi, F.R. Jensen, P.T. Hammond, Hemostatic multilayer coatings, Adv. Mater. 24 (2012) 492–496.
[48] A. Sasidharan, L.S. Panchakarla, A.R. Sadanandan, A. Ashokan, P. Chandran, C.M. Girish, D. Menon, S.V. Nair, C.N. Rao, M. Koyakutty, Hemocompatibility and macrophage response of pristine and functionalized graphene, Small 8 (2012) 1251–1263.
[49] S. Kattula, J.R. Byrnes, A.S. Wolberg, Fibrinogen and fibrin in hemostasis and thrombosis, Arterioscler. Thromb. Vasc. Biol. 37 (2017) e13–e21.